Pharmacogn J. 2026; 18(1): 8-17
A Multifaceted Journal in the field of Natural Products and Pharmacognosy
www.phcogj.com

Original Article

LC–MS Profiling, In Silico Docking–MD and ADMET of *Uncaria gambir Roxb*. for p38 MAPK Inhibition

Yudi Ambeng[1]*, Nia Kania[2], Ika Kustiyah Oktaviyanti[2], Eka Yudha Rahman[3]

ABSTRACT

Introduction: p38 mitogen-activated protein kinase (MAPK) is a pivotal regulator of inflammatory and cancer pathways. This study investigates phytochemicals from Bajakah (*Uncaria gambir* Roxb.) bark as potential p38 MAPK inhibitors, integrating LC–MS profiling with computational drug discovery. **Methods:** Bajakah bark extract was profiled by liquid chromatography–high-resolution mass spectrometry (LC–HRMS) to identify major phytochemicals. Promising non-toxic candidates were selected via in silico toxicity prediction (ProTox-II) and ADME assessment (pkCSM). Molecular docking against p38 MAPK (PDB ID: 3QUE) was performed using AutoDock Vina, followed by 50 ns molecular dynamics simulations with GROMACS and MM/PBSA binding free energy calculations using gmx_MMPBSA. **Results:** LC–HRMS identified ten major phytochemicals; 8-methylnaphthalene-1,2-diol (Diol) and methyl cinnamate exhibited non-toxic profiles (LD_{50} > 2,600 mg/kg; no CYP450 liabilities) with favorable ADME properties. Molecular docking revealed binding energies of −8.04 kcal/mol (Diol), −11.4 kcal/mol (Skepinone-L reference), and −6.4 kcal/mol (methyl cinnamate). Both Diol and Skepinone-L engaged conserved hydrophobic residues (VAL38 and LYS53), with Diol showing additional engagement at LEU104, and docking RMSD validation within 2.5 Å. Molecular dynamics confirmed stable Diol–p38 complex binding (RMSD ~0.30 nm), with balanced solvent accessibility, stable dynamic binding dominated by electrostatic interactions, and adaptive conformational sampling. MM/PBSA analysis revealed binding free energies of −21.9 kcal/mol (Diol) and −32.9 kcal/mol (Skepinone-L), with Diol's affinity driven by electrostatic interactions (−29.62 kcal/mol). **Conclusions:** 8-Methylnaphthalene-1,2-diol emerges as a promising natural p38 MAPK inhibitor candidate with favorable safety profiles and dynamic binding properties, warranting biochemical validation and structure–activity relationship optimization.

Keywords: 8-methylnaphthalene-1,2-diol, bajakah, computational modeling, drug discovery, molecular docking, phytochemical profiling

Yudi Ambeng[1]*, Nia Kania[2], Ika Kustiyah Oktaviyanti[2], Eka Yudha Rahman[3]

[1]*Department of Urology, dr. Doris Sylvanus General Hospital, Medical Faculty, Palangka Raya University, Palangka Raya, Center Kalimantan, INDONESIA.*

[2]*Department of Pathology, Ulin General Hospital, Medical Faculty, Lambung Mangkurat University, Banjarmasin, South Kalimantan, INDONESIA.*

[3]*Department of Urology, University of Lambung Mangkurat, Banjarmasin, INDONESIA.*

Correspondence

Y. Ambeng

Department of Urology, dr. Doris Sylvanus General Hospital, Medical Faculty, Palangka Raya University, Palangka Raya, Center Kalimantan, INDONESIA.

E-mail: yudi.ambeng.ya@gmail.com

History

- Submission Date: 13-11-2025;
- Review completed: 02-12-2025;
- Accepted Date: 21-01-2026.

DOI : 10.5530/pj.2026.18.111

Article Available online

http://www.phcogj.com/v18/i1

INTRODUCTION

Indonesia is a country with the largest biodiversity of animals and plants in the world. These animals and plants have been utilized for various purposes including for medicine, such as kweni mango fruit (*Mangifera odorata*), kelakai leaves (*Stenochlaena palustris*), black cumin (*Nigella sativa*), pikajar (*Schizaea digitata*), dayak onion (*Eleutherine palmifolia*), and longjack (*Eurycoma longifolia Jack*), ramania (*Bouea macrophylla Griff*), and bajakah kalalawit (*Uncaria gambir Roxb*)[1–7].

Bajakah Kalalawit is a plant known since ancient times by the people of Kalimantan as a medicinal plant that has many properties[8]. Bajakah wood extract contains catechins, phenolics, flavonoids, tannins, and saponins believed to prevent heart disease, obesity, diabetes, and proven to increase collagen formation[9]. Bajakah can also help the wound healing process and treat several other diseases[10,11]. Various studies have been conducted to evaluate the use of anti-proliferative and pro-apoptotic substances in treating cancer. Secondary metabolites in some bajakah kalalawit have certain biological properties such as catechins and proanthocyandidin that have the potential to be developed into cancer treatment modalities, especially prostate cancer[12].

The mechanism of prostate cancer cell development, the p38 MAPK pathway plays an important role in regulating prostate cell growth. Previous research has revealed that protaapigenone, a flavonoid-derived compound, can suppress the development of cancer cells through the activation of the p38 MAPK pathway[13]. Research by Erdogan et al also states that flavonoid-derived compounds, namely flavone apigenin, can inhibit the p38 MAPK pathway so that the development of prostate cancer cells can be suppressed[14]. In this regard, many studies explore natural resources to find new compounds as anticancer with the target of inhibiting p38 MAPK.

Edyson et al research has identified chatecin found in bajakah leaves and twigs. However, the identification of phytochemical compound on bajakah bark has never been done. Therefore, this study will identify the phytochemical profile of bajakah bark extract with LC- MS and the interaction between phytochemical compounds with p38 MAPK in silico[6].

MATERIALS AND METHODS

Phytochemical Profile

Uncaria gambir Roxb samples were collected in Seruyan Village, Seruyan Raya Sub-district, Seruyan Regency, Central Kalimantan (2°26′30.674″ N, 112°25′14.394″ E) and authenticated at the Integrated Laboratory of Lambung Mangkurat University, South Kalimantan, on March 27, 2024. The hanging roots were cut into small pieces to separate the plant material into cambium and stem

Cite this article: Yudi A, Nia K, Ika K O, Eka Y R. LC–MS Profiling, In Silico Docking–MD and ADMET of *Uncaria gambir Roxb.* for p38 MAPK Inhibition. Pharmacogn J. 2026;18(1): 8-17.

bark. The stem bark was macerated with ethanol, and the filtrate was concentrated and freeze-dried at −50 °C to yield 175 g of dry powder. This powder was dissolved in methanol, filtered, and analyzed by liquid chromatography–high-resolution mass spectrometry (LC–HRMS) using a C18 column with 0.1% formic acid mobile phase at 0.2 mL/min over 25 minutes[15].

Identified phytochemical components underwent in silico toxicity and pharmacokinetic predictions. Target-organ toxicity (hepatic, neurological, cardiac, and respiratory) was assessed via the ProTox-II web server, while absorption, distribution, metabolism, and excretion (ADME) parameters were predicted using the pkCSM platform.

LD50 and Toxicity prediction

Toxicity prediction is very important to determine the toxic properties of compounds to target organs, such as hepatic, neuro, cardiac and respiratory. Prediction of toxicity to target organs uses a web-based application https://tox-new.charite.de/protox_II/index.php?site=home which can be accessed online[16].

Pharmacokinetics Prediction

Pharmacokinetic predictions include absorption, distribution, metabolism and excretion (ADME). These predictions are very important in drug discovery and development. ADME prediction utilizes a web-based application, https://biosig.lab.uq.edu.au/pkcsm/, which can be accessed online[16,17].

Ligand and Protein preparation

For this study, the crystal structure of Mitogen-Activated Protein Kinase 3 (MAPK3) (PDB ID: 3QUE) was obtained from https://www.rcsb.org/. Structure preparation in PyMOL and AutoDockTools involved removing bound ligand and crystallographic water, adding polar hydrogens, and repairing incomplete residues. The processed structure was saved in PDB format and converted to PDBQT for docking analysis[18,19].

Ligands selected included Skepinone-L as the positive control (CID: 45279963), 8-Methylnaphthalene-1,2-diol (CID: 656869), and methyl cinnamate (CID: 637520). Their 3D structures were downloaded from https://pubchem.ncbi.nlm.nih.gov/ in SDF format, geometry-optimized using Open Babel with the --gen3d option, then converted to PDB and subsequently to PDBQT using AutoDockTools[18].

Molecular Docking

Molecular docking was performed using AutoDock Vina version 23d1252-mod, with the grid box centered on the native ligand site at coordinates X = 3.153, Y = 1.476, Z = 22.961 and dimensions of 20 × 20 × 20 Å^3. The exhaustiveness was set to 16, selected to balance computational efficiency and docking accuracy for rigid receptor protocols. Binding poses were evaluated based on predicted binding affinity[18].

Post-docking analysis identified optimal poses based on lowest binding energy and RMSD relative to the native ligand. Interaction analysis was carried out in PyMOL and BIOVIA Discovery Studio Visualizer, highlighting hydrogen bonding, hydrophobic interactions, π–π stacking, and positional overlap with the native ligand binding site[19,20].

Molecular Dynamics Simulation

The p38 MAPK structure (PDB: 3QUE) was processed using GROMACS 2023.3 with AMBER99SB-ILDN force field and TIP3P water model[21–23]. Ligands (Skepinone-L and 8-Methylnaphthalene-1,2-diol) were parameterized using GAFF with AM1-BCC charges via ACPYPE[24]. Systems were solvated in a dodecahedral water box (1.0 nm buffer) and neutralized with 0.15 M NaCl. Energy minimization was performed using the steepest descent algorithm. NVT equilibration was conducted at 300 K using the V-rescale thermostat (τ = 0.1 ps), followed by NPT equilibration at 1 bar using the Parrinello–Rahman barostat (τ = 2.0 ps, compressibility 4.5 × 10^{-5} bar^{-1}). Short-range van der Waals and Coulomb interactions were treated with a 1.0 nm cutoff, while long-range electrostatics were handled using the Particle Mesh Ewald (PME) method. Production MD simulations were run for 50 ns with a 2 fs timestep using LINCS constraints[25–27]. Coordinates were saved every 10 ps for subsequent analysis.

Structural Analysis

Trajectory analyses used standard GROMACS utilities including RMSD/RMSF for stability assessment, radius of gyration for protein compactness, SASA for solvent exposure, and hydrogen bond analysis for intra-protein and protein-ligand interactions. Principal component analysis was conducted on Cα atoms using covariance matrix diagonalization to characterize conformational sampling patterns**.** Visual inspection was performed using PyMOL and Discovery Studio Visualizer[19,20].

Binding Free Energy Analysis

MM/PBSA calculations were performed using gmx_MMPBSA with 200 snapshots extracted every 250 ps from the final 20 ns of each 50 ns trajectory[28]. Binding free energy components included molecular mechanics energy (van der Waals + electrostatic), polar solvation (Poisson-Boltzmann), and non-polar solvation (SASA-based). Per-residue decomposition identified key binding hotspots.

RESULTS AND DISCUSSION

Phytochemical Profile

The collection of bajakah kalalawit in Seruyan Village, Seruyan Raya District, Seruyan Regency, Central Kalimantan (2o26'30.674 NL-112o25'14.394 EL) as shown in the Figure 1.

The phytochemical profile of the separation results by LCHR-MS has been obtained according to Table 1. In the table 1, 10 compounds with the highest area (%) were selected.

Based on Table I, it appears that bajakah bark extract contains tetralin compounds with the largest area. This area is proportional to the concentration of the compound. Research by Shafee et al mentioned that tetralin has the potential as an anticancer by inhibiting Hela cells and inhibiting MCF7 breast cancer cells [29]. Besides tetralin, bajakah bark extract also contains 4- Phenylbutyric acid. This compound can protect nerve cells and endoplasmic reticulum stress [30].

LD50 and Toxicity prediction

Toxicity prediction includes predicting the toxicity of a substance to target organs, such as the liver, nerves, kidneys, heart, and respiratory system. In addition, toxicity is determined by the LD50, which is the minimum dose that causes 50% mortality. LD50 and toxicity prediction are presented in Table 2.

Based on Table 2, there are two compounds that have the potential to be developed as drugs because they are not toxic to organs. The compounds are Methyl cinnamate and 8- Methylnaphthalene-1,2-diol (Figure 2).

The results of the study are in accordance with previous research which states that oral administration of tablets containing α-mangosteen, piperine, curcumin, methyl cinnamate and vitamins in rats acutely did not cause toxicity in various organs [31]. Meanwhile, 8-Methylnaphthalene-1,2-diol until now no one has mentioned the toxic properties of the compound. Thus, for ADME analysis and molecular docking, only those two compounds that have been proven safe and non-toxic are used.

Table 1. Ten phytochemical compounds of bajakah bark extracts

No	Name	CID	MW	RT (min)	Area (%)	Isomeric SMILES
1	Tetralin	8404	132.0937	6.179	24.513	C1CCC2=CC=CC=C2C1
2	4-Phenylbutyric acid	4775	164.0837	19.332	21.429	C1=CC=C(C=C1)CCCC(=O)O
3	(+/-)-Camphoric acid	21491	200.1046	1.837	15.397	CC1(C(CCC1(C)C(=O)O)C(=O)O)C
4	Cuminaldehyde	326	148.0886	4.527	13.216	CC(C)C1=CC=C(C=C1) C=O
5	(2E)-decenoic acid	5282724	170.1299	9.238	10.345	CCCCCCC/C=C/C(=O)O
6	hymecromone	5280567	176.0471	6.89	4.330	CC1=CC(=O)OC2=C1C= CC(=C2)O
7	Methyl cinnamate	637520	162.0679	5.792	4.072	COC(=O)/C=C/C1=CC=CC=C1
8	(E)-Ferulic acid	445858	194.0578	4.216	3.933	COC1=C(C=CC(=C1)/C= C/C(=O)O)O
9	N-Glycosyl-L- asparagine	440002	294.1059	0.789	2.114	C([C@@H]1[C@H]([C@@H]([C@H]([C@@H]
10	8- Methylnaphthalene- 1,2-diol	656869	174.068	174.068	2.114	CC1=C2C(=CC=C1)C=C C(=C2O)O

Table 2. LD50 and prediction toxicity

No.	Compound	Oral Rat Acute Toxicity LD50 (mg/kg)	Organ Toxic				
			Hepato toxic	Neuro toxic	Nephrot oxic	Cardio toxic	Respiratory toxic
1	Tetralin	6700	No	Yes	No	No	No
2	4-Phenylbutyric acid	1000	No	No	Yes	Yes	No
3	(E)-Ferulic acid	1772	No	No	Yes	No	No
4	Cuminaldehyde	1320	No	Yes	No	No	No
5	(2E)-decenoic acid	1925	Yes	No	No	No	No
6	Hymecromone	2850	No	No	No	No	Yes
7	Methyl cinnamate	2610	No	No	No	No	No
8	(+/-)-Camphoric acid	3250	No	No	No	No	Yes
9	N-Glycosyl-L- asparagine	1190	No	Yes	No	No	Yes
10	8- Methylnaphthale ne-1,2-diol	400	No	No	No	No	No

Table 3. Summary of binding energy values (in kcal/mol)

Ligand	Binding Energy (kcal/mol)	Favourable Bond	Unfavourable Bond	Note
Skepinone (control)	−11.4	VAL30, VAL38, ALA51, LYS53, ILE84, LEU108, LEU167, LEU171, LEU104, VAL105, ASP168, ASN115, HIS174, THR175	ASP176	Very strong
8-Methylnaphthalene-1,2-diol	−8.035	VAL38, LYS53, LEU 75, ILE 84, LEU 104,	-	Strong
Methyl cinnamate	−6,4	LYS 53, ILE 84, LEU 104	-	Weak

Table 4. ADME Methyl cinnamate dan 8-Methylnaphthalene-1,2-diol

No	Parameter	Unit	Methyl cinnamate	8-Methylnaphthalene- 1,2-diol
	Absorpsion			
1	• Caco2 permeability	Numeric (log Papp in 10^{-6} cm/s)	1.442	1.653
	• Human Intestinal Absorpsition	Numeric (% Absorbed)	97.453	91.598
	Distribution			
2	• VDss (human)	Numeric (log L/kg)	-0.001	0.294
	• BBB permeability	Numeric (log BB)	0.238	0.529
	Metabolism			
3	• CYP2D6 substrate	Categorical (Yes/No)	No	No
	• CYP3A4 substrate	Categorical (Yes/No)	No	No
	Excretion			
4	Total Clearance	Numeric (log ml/min/kg)	0.814	0.16
	Renal OCT2 substrate	Categorical (Yes/No)	No	No

Table 5. MM/PBSA energy component breakdown

Component	Diol (kcal/mol)	Skepinone (kcal/mol)	Interpretation
VDWAALS	−22.28	−48.15	Skepinone shows stronger van der Waals interactions
EEL	−29.62	−18.14	Diol exhibits stronger electrostatic contributions
EPB	32.03	37.15	Both show similar polar solvation penalties
ENPOLAR	−2.04	−3.81	Comparable non-polar solvation contributions
TOTAL	**−21.90**	**−32.95**	Skepinone demonstrates superior overall binding

MM/PBSA energy component breakdown, (VDWAALS: van der Waals; EEL: Electrostatic; EPB: Polar solvation; ENPOLAR: Non-polar solvation)

Figure 1. Kalalawit bajakah sampling area

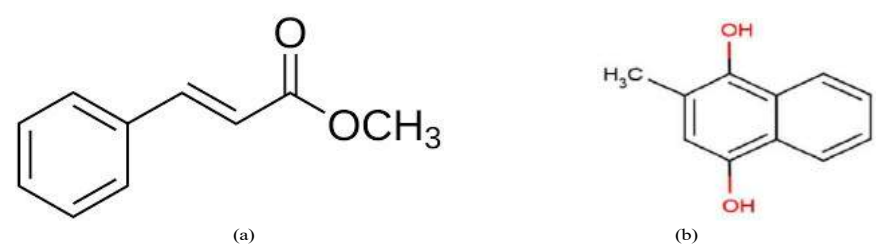

Figure 2. Molecular structures of (a) Methyl cinnamate and (b) 8-Methylnaphthalene-1,2-diol

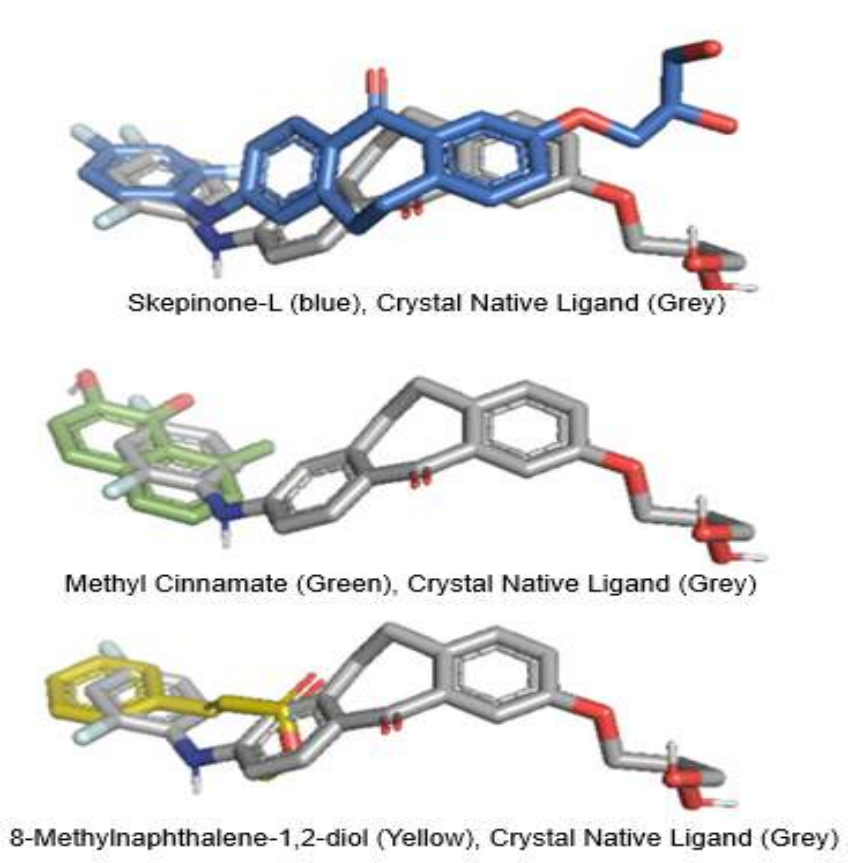

Figure 3. Stacking visualization to determine the binding pocket position on the three ligands

Molecular Docking

Binding Energy Affinity

The binding energy between the ligand and p38 MAPK is expressed in Vina scores as presented in Table 3.

The binding energy for 8-Methylnaphthalene-1,2-diol against p38 MAPK (–8.035 kcal/mol) is close but slightly weaker than that of the native inhibitor Skepinone-L (–11.4 kcal/mol), reflecting strong affinity despite the absence of hydrogen bonds. Both ligands interact primarily via favourable hydrophobic contacts in the same binding pocket, particularly involving VAL38, LYS53, ILE84, and LEU104, consistent with effective kinase inhibition. These polyphenolic scaffolds are recognized modulators of MAPKs and p38, influencing cellular proliferation and apoptosis through signal transduction pathways [32].

RMSD Validation/Docking Re-evaluation

The RMSD value obtained for the redocked Skepinone pose was 2.376 Å, which is slightly above the commonly accepted accuracy threshold of 2 Å for docking validation. However, literature indicates that RMSD values up to 2.5 Å are still considered acceptable and reliable for reproducing experimental ligand poses in protein–ligand docking studies. Therefore, the docking process for Skepinone is judged to be successful and appropriate for further analysis [33].

Pose Validation and Binding Pocket

All ligands show binding to the same active site as skepinone. As shown in the following figure 3.

The ligand orientations demonstrated excellent convergent stacking, particularly during initial docking runs with exhaustiveness set to 16. Re-docking validation procedures provided comprehensive 3D structural alignment and detailed 2D. The interactions between the p38 MAPK protein and the native ligands Skepinone-L (CID: 45279963), Methyl cinnamate (CID: 637520), and 8-Methylnaphthalene-1,2-diol (CID:656869) are shown in Figure 4.

The docking results revealed that 8-Methylnaphthalene-1,2-diol engages in robust Pi interactions with Lys-53—one of the key residues involved in native ligand binding—and additionally forms a hydrogen bond with Leu-104, consistent with its strong binding energy. In contrast, methyl cinnamate exhibited predominantly weaker Pi contacts, reflecting its lower docking score.

In summary, 8-Methylnaphthalene-1,2-diol demonstrates promising potential as a MAPK3 inhibitor based on its favorable docking score and pose validation, whereas methyl cinnamate, despite showing weaker binding affinity, maintains a valid orientation that supports its inclusion in docking analyses. These docking outcomes provide a solid foundation for subsequent molecular dynamics simulations to assess the dynamic stability of the ligand–protein complexes under physiological conditions.

ADME Analysis

ADME analysis includes absorption, distribution, metabolism and excretion. The ADME results for Methyl cinnamate and 8-Methylnaphthalene-1,2-diol are presented in Table 4.

Absorption of both compounds is very good. This is seen from the Caco2 permeability value which has a prediction above 0.9. Caco-2 is an in vitro model of the human intestinal mucosa to predict the absorption of orally administered drugs. Although both compounds have good absorption ability, 8-Methylnaphthalene-1,2-diol is still better than Methyl cinnamate. In addition to Caco2 permeability, absorption is also assessed from human intestinal absorption, which predicts the proportion of compounds absorbed (>30%) through the human small intestine. The human intestinal absorption of Methyl cinnamate and 8-Methylnaphthalene-1,2- diol was very good, but Methyl cinnamate was better.

The steady state volume of distribution (VDss) value of 8-Methylnaphthalene-1,2-diol compound is better than Methyl cinnamate. VDss is the theoretical volume required to distribute the drug to give the same concentration as in blood plasma. VDss is considered low if below 0.71 L/kg (log VDss < 0.15) and high if above 2.81 L/kg (log VDss > 0.45). Meanwhile, the blood-brain barrier (BBB) permeability value of 8-Methylnaphthalene-1,2-diol compound is better than Methyl cinnamate. BBB permeability is the ability of a drug to penetrate the brain to help reduce side effects and toxicity, or to increase the pharmacological activity of the compound in the brain.

Both compounds Methyl cinnamate and 8-Methylnaphthalene-1,2-diol are not substrates of cytochrome P450 enzymes. Cytochrome P450 is a large family of hemeprotein- type enzymes that function as oxidizing catalysts in the metabolic pathways of steroids, fatty acids, xenobiotics, including drugs, toxins and carcinogens. Various organic chemical reactions are accelerated by CYPs, such as monooxygenation, peroxidation, reduction, dealkylation, epoxidation and dehalogenation reactions. These reactions are specifically aimed at converting substrate compounds into polar metabolites for excretion or processed by other enzymes in phase II metabolism into conjugate compounds [34].

Total Clearance is a pharmacokinetic parameter that describes the length of time a drug remains in the blood. It is related to the systemically available dose, and it is important to determine the dose level to achieve a stable concentration. Meanwhile, Renal OCT2 substrate indicates a major transporter located in the basolateral membrane of the renal proximal tubule. This transporter plays an important role in the active secretion of cationic drugs into the urine.

Molecular Dynamic

Structural Stability and Conformational Dynamics

RMSD analysis (Figure 5a) showed system equilibration within 10 ns. Apo p38 MAPK fluctuated around 0.20 nm, while Diol-bound (~0.30 nm) and Skepinone-bound (~0.22 nm) systems demonstrated stable binding. The RMSD profile of Diol reflects moderate but controlled flexibility, consistent with reports that adaptive dynamics in kinase inhibitors can confer selectivity advantages and reduce resistance development[35]. Radius of gyration remained consistent (2.24-2.28 nm) across systems (Figure 5b), indicating preserved protein compactness[36].

SASA measurements revealed balanced solvent accessibility for Diol-bound complexes (170-185 nm^2), while Skepinone-bound systems showed greater compaction (160-175 nm^2) and apo systems highest exposure (175-185 nm^2) (Figure 6a). Internal hydrogen bonding remained stable (Diol: 240-280 bonds; Skepinone: 235-275 bonds) (Figure 6b), confirming secondary structure preservation throughout simulations. This stability profile aligns with studies showing that natural product inhibitors often maintain favorable dynamic properties while providing therapeutic effects[37,38].

Principal Component Analysis and Adaptive Binding

PCA revealed significant conformational sampling differences. Diol-bound complexes demonstrated broader sampling along PC1 (±7 nm) compared to Skepinone (±4 nm) and apo systems (±5 nm) (Figure 7a-b). This enhanced conformational exploration suggests adaptive binding capability that may accommodate different p38 MAPK activation states. Recent investigations emphasize that inhibitors with moderate flexibility can exhibit improved selectivity profiles by accommodating conformational changes in kinase domains [39]. The intermediate flexibility observed with Diol may provide advantages

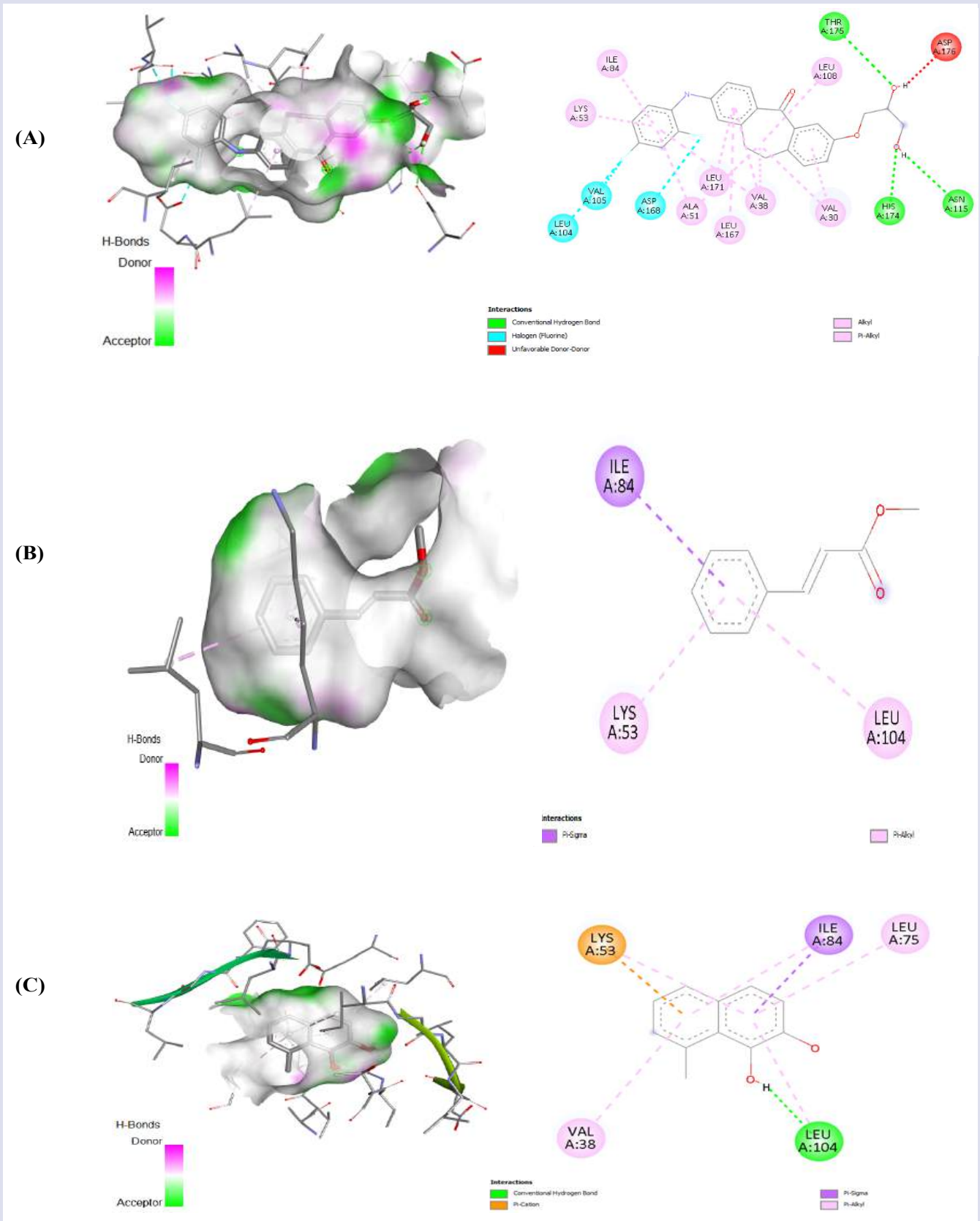

Figure 4. p38 MAPK interaction with (a) Skepinone-L (CID: 45279963); (b) 8-Methylnaphthalene-1,2-diol (CID: 656869); (c) Methylcinnamate (CID: 637520)

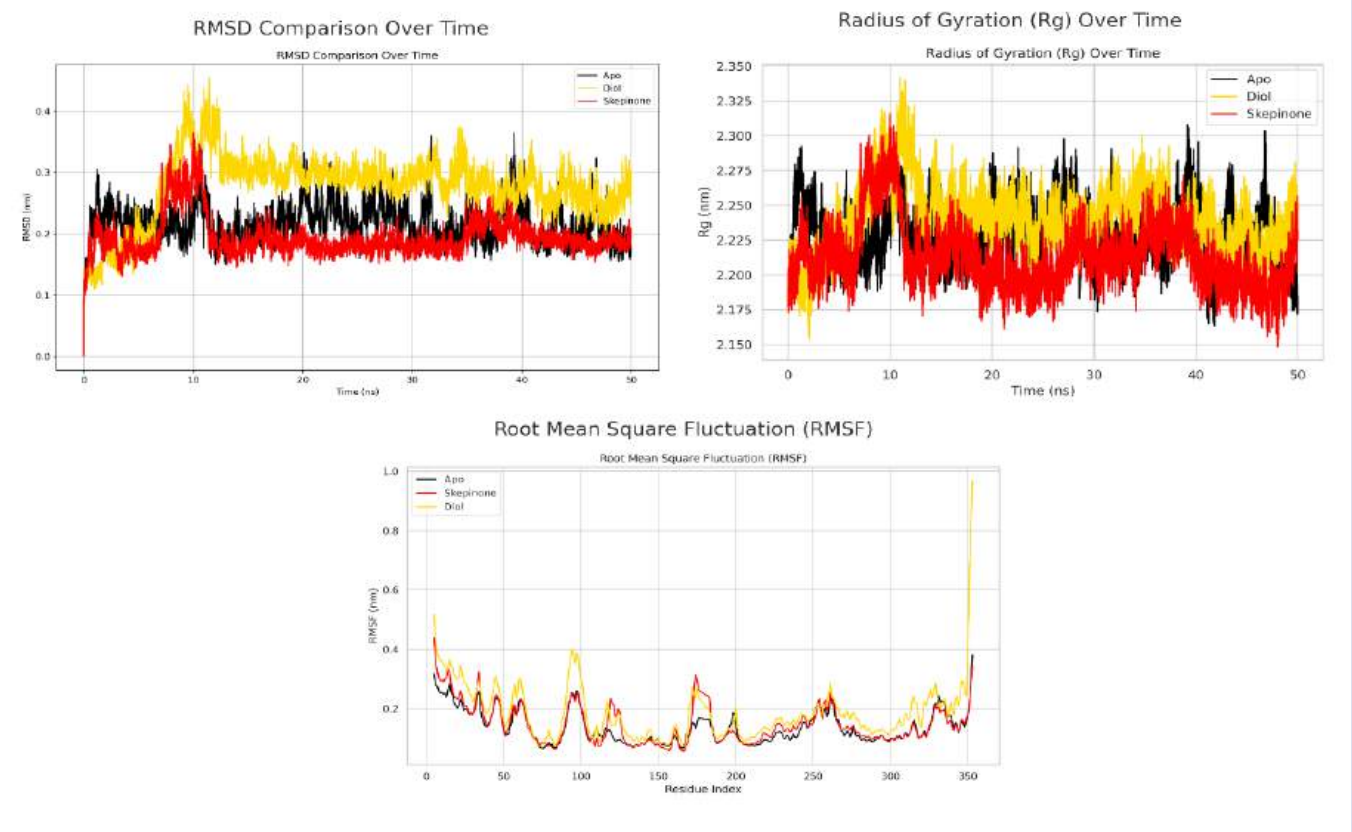

Figure 5. Structural stability of p38 MAPK complexes. (a) RMSD over 50 ns MD simulations; (b) radius of gyration; (c) residue-wise RMSF. Apo (black), Diol (gold) and Skepinone-L (red).

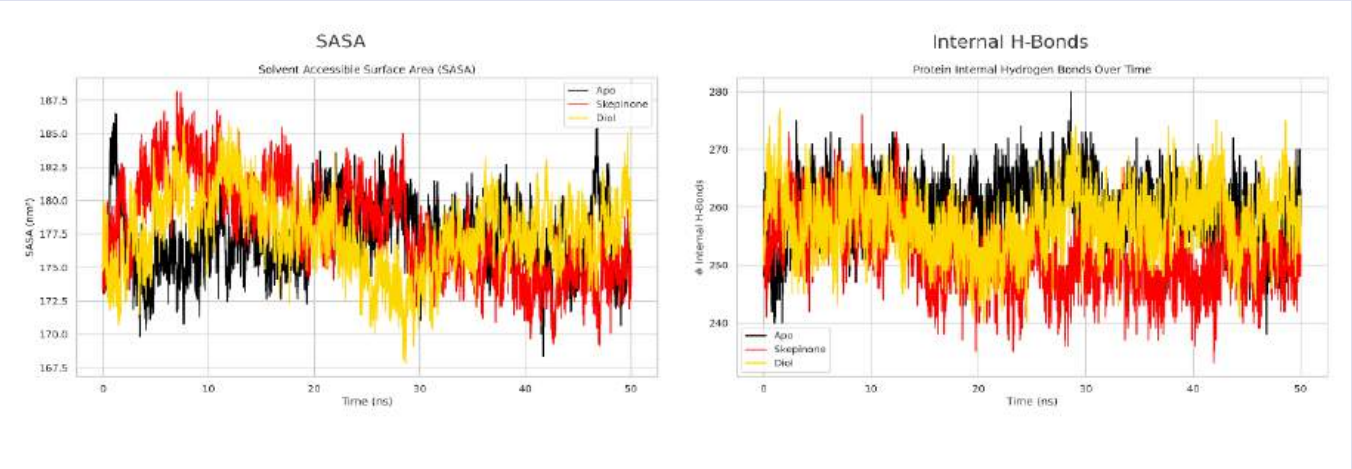

Figure 6. Solvent exposure and internal hydrogen bonding. (a) Solvent-accessible surface area versus time; (b) number of intramolecular hydrogen bonds

for targeting both active and inactive conformations while reducing resistance potential[40].

Binding Energetics and Mechanistic Insights

MM/PBSA calculations yielded binding free energies of -21.90 kcal/mol (Diol) and -32.95 kcal/mol (Skepinone-L). Per-residue MM/PBSA decomposition values represent averaged total binding energy contributions calculated over the selected trajectory frames and include combined van der Waals and electrostatic components. Energy decomposition revealed distinct mechanisms: Diol achieved binding through stronger electrostatic interactions (-29.62 vs -18.14 kcal/mol for Skepinone), while Skepinone relied on superior van der Waals interactions (-48.15 vs -22.28 kcal/mol for Diol) (Table 5; Figure 8). This electrostatic-dominated binding pattern is notable, as studies demonstrate that direct electrostatic interactions often play a dominant role over hydrophobic interactions in selective protein-ligand recognition[41].

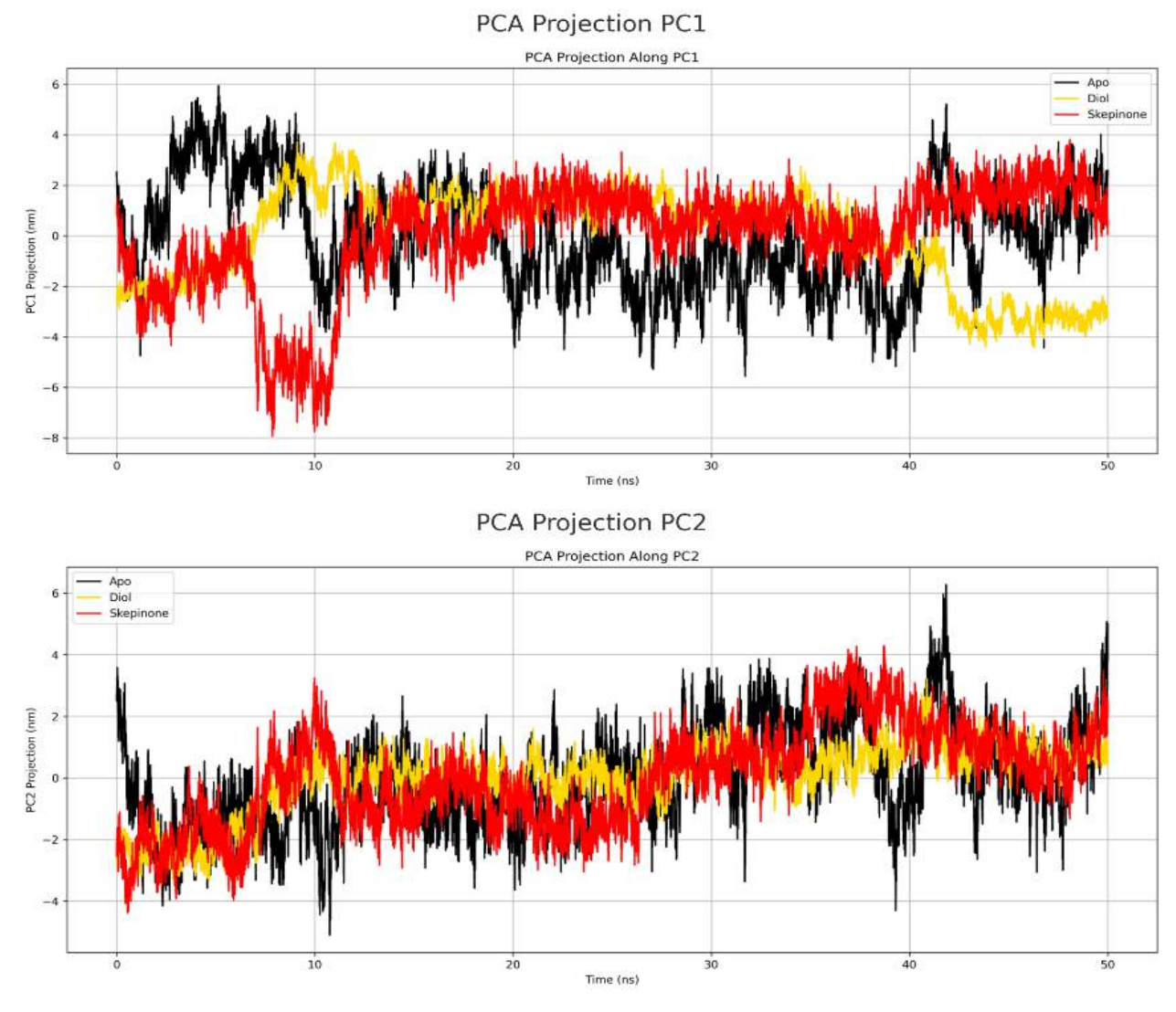

Figure 7. Principal component projections. (a) PC1 and (b) PC2 projections of Apo, Diol and Skepinone-bound trajectories over 50 ns. Diol covers a broader conformational space than Skepinone.

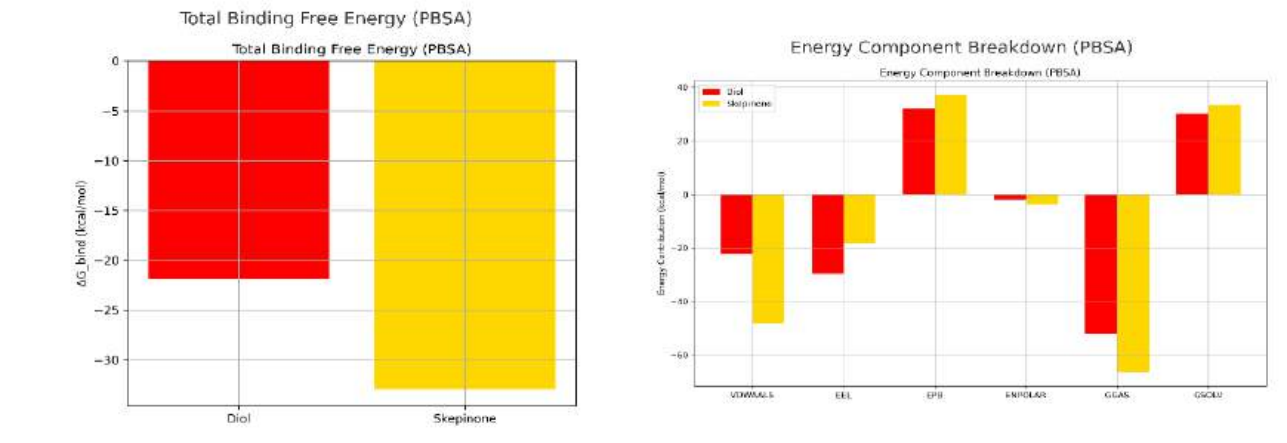

Figure 8. Total binding free energy and energy component breakdown. (a) Delta total binding free energy between Diol and Skepinone; (b) Energy Component Breakdown between Diol and Skepinone

The predominance of electrostatic interactions for Diol suggests enhanced selectivity potential, as hydrogen bonding patterns are more specific than hydrophobic interactions due to directional constraints [42,43]. Per-residue decomposition identified VAL38 as a critical shared hotspot (Diol: -1.05 kcal/mol; Skepinone: -1.12 kcal/mol), confirming ATP-competitive inhibition mechanism. This conserved interaction validates the binding site while the distinct energetic profiles suggest orthogonal selectivity patterns that may reduce off-target effects.

Despite moderate binding affinity compared to synthetic inhibitors, Diol's distinct electrostatic mechanism, favorable dynamic properties, and predicted safety profile distinguish it from current therapeutic options[44,45]. The traditional use validation from Bajakah provides additional confidence for clinical advancement[46,47]. Priority experimental studies should include enzymatic activity assays, cell-based efficacy testing, kinome selectivity profiling, and pharmacokinetic validation to confirm computational predictions[48,49].

The integration of computational drug discovery with traditional medicinal knowledge represents an optimal approach for natural product development. The comprehensive analysis provides clear hypotheses for experimental testing and structure-based optimization strategies that could significantly enhance binding affinity while preserving favorable characteristics[50].

CONCLUSION

The integrated LC–MS phytochemical profiling and in silico assessments identified 8-methylnaphthalene-1,2-diol as a promising p38 MAPK inhibitor, combining non-toxic ADMET properties with strong docking affinity (–8.04 kcal/mol) and stable binding dynamics. Molecular dynamics and MM/PBSA analyses highlighted its favorable electrostatic-driven binding and dynamic adaptability within the kinase active site. Methyl cinnamate, despite lower affinity, displayed acceptable ADME and valid binding orientation. These findings provide a robust computational foundation for further experimental validation, including enzyme inhibition assays, cell-based studies, and medicinal chemistry optimization to develop novel, selective p38 MAPK inhibitors from natural polyphenolic scaffolds.

REFERENCES

1. Mashuri, Noor Z, Suhartono eko, et al. Trends on Pharmacological Activity of Mangifera Odorata Research: Bibliometric Study 2014-2024. Pak J Life Soc Sci.
2. Suhartono E, Muthmainah N, Marisa D, et al. Protective Role of Kelakai (Stenochlaena Palustris) Extract on Malathion-induced Genotoxic: FTIR Spectroscopy Study. INTERNATIONAL JOURNAL OF DRUG DELIVERY TECHNOLOGY 2022; 12: 15–18.
3. Oktaviyanti IK, Nurrasyidah I., Muthmainah N., et al. Supplementation of Nigella sativa as Antioxidant in COVID-19 Patients: In silico Study via the Nrf2-Keap1 Pathway. INTERNATIONAL JOURNAL OF DRUG DELIVERY TECHNOLOGY 2022; 12: 1028–1032.
4. Firmanul Arifin Y, Suhartono E, Hamidah S. Relationship between growth sites and content of steroids and sterols from Pikajar (Schizaea digitata). IOP Conf Ser Earth Environ Sci 2020; 528: 012030.
5. Biworo A, Abdurrahim, Nupiah N, et al. The effect of dayak onion (Eleutherine palmifolia (L.) merr) tuber extract against erythema and melanin index on rat (Rattus norvegicus) skin induced by acute UV. 2019, p. 020036.
6. Edyson, Pardede AME, Nugraha HG, et al. In vivo antioxidant and UV-photoprotective of extract pasak bumi (Eurycoma Longifolia Jack.). 2019, p. 020029.
7. Taufiqurrahman I, Gupita SHN, Oktiani BW, et al. The Effect of Ramania Leaves Extract Gel (Bouea macrophylla Griff) on the Number of Osteoblast (in vivo Study of Post Extraction in Wistar Rats (Rattus norvegicus)). Pharmacognosy Journal 2024; 15: 1219–1223.
8. Alhawaris. Potency of Borneo Endemic and Typical Plants as AntiCancer Medicines. Jurnal Kesehatan Pasak Bumi Kalimantan;5.
9. Aprely KJ, Misfadhila S, Asra R. A Review: The Phytochemistry, Pharmacology and Traditional Use of Gambir (Uncaria gambir (Hunter) Roxb) . EAS Journal of Pharmacy and Pharmacology.
10. Lismana L, Hendiani I, Herwanda H. The Effect of Bajakah Stem Extract on Bacterial Inhibitory Concentration and Wound Healing Process. 2022. Epub ahead of print 2022. DOI: 10.2991/ahsr.k.220302.013.
11. Diana Alexandra F, Frethernety A, Sri Martani N, et al. Oxidative Stress in Streptozotocin-Induced Rats and The Role of Bajakah (Uncaria Sp.) as Antioxidants. Asian Journal of Healthy and Science 2023; 2: 353–365.
12. Sung H, Ferlay J, Siegel RL, et al. Global Cancer Statistics 2020: GLOBOCAN Estimates of Incidence and Mortality Worldwide for 36 Cancers in 185 Countries. CA Cancer J Clin 2021; 71: 209–249.
13. Guicheux J, Lemonnier J, Ghayor C, et al. Activation of p38 Mitogen-Activated Protein Kinase and c-Jun-NH2-Terminal Kinase by BMP-2 and Their Implication in the Stimulation of Osteoblastic Cell Differentiation. Journal of Bone and Mineral Research 2003; 18: 2060–2068.
14. Erdogan S, Turkekul K, Dibirdik I, et al. Midkine silencing enhances the anti–prostate cancer stem cell activity of the flavone apigenin: cooperation on signaling pathways regulated by ERK, p38, PTEN, PARP, and NF-κB. Invest New Drugs 2020; 38: 246–263.
15. Beccaria M, Cabooter D. Current developments in LC-MS for pharmaceutical analysis. Analyst 2020; 145: 1129–1157.
16. Oktaviyanti IK, Nurrasyidah I., Muthmainah N., et al. Supplementation of Nigella sativa as Antioxidant in COVID-19 Patients: In silico Study via the Nrf2-Keap1 Pathway. INTERNATIONAL JOURNAL OF DRUG DELIVERY TECHNOLOGY 2022; 12: 1028–1032.
17. Rachmawati R, Idroes R, Suhartono E, et al. In Silico and In Vitro Analysis of Tacca Tubers (Tacca leontopetaloides) from Banyak Island, Aceh Singkil Regency, Indonesia, as Antihypercholesterolemia Agents. Molecules 2022; 27: 8605.
18. Trott O, Olson AJ. AutoDock Vina: Improving the speed and accuracy of docking with a new scoring function, efficient optimization, and multithreading. J Comput Chem 2010; 31: 455–461.
19. Schrödinger L. The PyMOL Molecular Graphics System, Version 2.5. Schrödinger, LLC.
20. BIOVIA. Discovery Studio Visualizer v2025. San Diego: Dassault Systèmes . BIOVIA Corp.
21. Abraham MJ, Murtola T, Schulz R, et al. GROMACS: High performance molecular simulations through multi-level parallelism from laptops to supercomputers. SoftwareX 2015; 1–2: 19–25.
22. Lindorff-Larsen K, Piana S, Palmo K, et al. Improved side-chain torsion potentials for the Amber ff99SB protein force field. Proteins: Structure, Function, and Bioinformatics 2010; 78: 1950–1958.
23. Jorgensen WL, Chandrasekhar J, Madura JD, et al. Comparison of simple potential functions for simulating liquid water. J Chem Phys 1983; 79: 926–935.
24. Sousa da Silva AW, Vranken WF. ACPYPE - AnteChamber PYthon Parser interfacE. BMC Res Notes 2012; 5: 367.
25. Bussi G, Donadio D, Parrinello M. Canonical sampling through velocity rescaling. J Chem Phys; 126. Epub ahead of print 7 January 2007. DOI: 10.1063/1.2408420.
26. Darden T, York D, Pedersen L. Particle mesh Ewald: An N ·log(N) method for Ewald sums in large systems. J Chem Phys 1993; 98: 10089–10092.

27. Hess B, Bekker H, Berendsen HJC, et al. LINCS: A linear constraint solver for molecular simulations. J Comput Chem 1997; 18: 1463–1472.
28. Valdés-Tresanco MS, Valdés-Tresanco ME, Valiente PA, et al. gmx_MMPBSA: A New Tool to Perform End-State Free Energy Calculations with GROMACS. J Chem Theory Comput 2021; 17: 6281–6291.
29. Shafiee F, Sadeghi-aliabadi H, Hassanzadeh F. Evaluation of cytotoxic effects of several novel tetralin derivatives against Hela, MDA-MB-468, and MCF-7 cancer cells. Adv Biomed Res 2012; 1: 76.
30. Mimori S, Okuma Y, Kaneko M, et al. Protective Effects of 4-Phenylbutyrate Derivatives on the Neuronal Cell Death and Endoplasmic Reticulum Stress. Biol Pharm Bull 2012; 35: 84–90.
31. Sari NK, Sriwidodo, Fauzi NI, et al. Acute toxicity test of tablets containing α-mangosteen, piperine, curcumin, methyl cinnamate and vitamin C in female wistar rats. Pharmacy Education 2024; 24: 158–162.
32. Vue B, Zhang S, Chen Q-H. Flavonoids with Therapeutic Potential in Prostate Cancer. Anticancer Agents Med Chem 2016; 16: 1205–1229.
33. Hubbard RE, Kamran Haider M. Hydrogen Bonds in Proteins: Role and Strength. In: Encyclopedia of Life Sciences. Wiley, 2010. Epub ahead of print 15 February 2010. DOI: 10.1002/9780470015902.a0003011.pub2.
34. Furge LL, Guengerich FP. Cytochrome P450 enzymes in drug metabolism and chemical toxicology: An introduction. Biochemistry and Molecular Biology Education 2006; 34: 66–74.
35. Baker ZD, Rasmussen DM, Levinson NM. Exploring the conformational landscapes of protein kinases: perspectives from FRET and DEER. Biochem Soc Trans 2024; 52: 1071–1083.
36. Assadieskandar A, Yu C, Maisonneuve P, et al. Effects of rigidity on the selectivity of protein kinase inhibitors. Eur J Med Chem 2018; 146: 519–528.
37. Zhou L, Zhang J, Zhao K, et al. Natural products modulating MAPK for CRC treatment: a promising strategy. Front Pharmacol; 16. Epub ahead of print 5 March 2025. DOI: 10.3389/fphar.2025.1514486.
38. Shi A, Liu L, Li S, et al. Natural products targeting the MAPK-signaling pathway in cancer: overview. J Cancer Res Clin Oncol 2024; 150: 6.
39. Araki M, Kamiya N, Sato M, et al. The Effect of Conformational Flexibility on Binding Free Energy Estimation between Kinases and Their Inhibitors. J Chem Inf Model 2016; 56: 2445–2456.
40. Smyth LA, Collins I. Measuring and interpreting the selectivity of protein kinase inhibitors. J Chem Biol 2009; 2: 131–51.
41. Scott AM, Antal CE, Newton AC. Electrostatic and Hydrophobic Interactions Differentially Tune Membrane Binding Kinetics of the C2 Domain of Protein Kinase Cα. Journal of Biological Chemistry 2013; 288: 16905–16915.
42. Gerber SH, Rizo J, Sudhof TC. Role of Electrostatic and Hydrophobic Interactions in Ca2+-Dependent Phospholipid Binding by the C2A-Domain From Synaptotagmin I. Diabetes 2002; 51: S12–S18.
43. Zuo W, Huang M-R, Schmitz F, et al. Probing Electrostatic and Hydrophobic Associative Interactions in Cells. J Phys Chem B 2024; 128: 10861–10869.
44. Banerjee A, Koziol-White C, Panettieri R. p38 MAPK inhibitors, IKK2 inhibitors, and TNFα inhibitors in COPD. Curr Opin Pharmacol 2012; 12: 287–292.
45. Ganguly P, Macleod T, Wong C, et al. Revisiting p38 Mitogen-Activated Protein Kinases (MAPK) in Inflammatory Arthritis: A Narrative of the Emergence of MAPK-Activated Protein Kinase Inhibitors (MK2i). Pharmaceuticals 2023; 16: 1286.
46. Pirintsos S, Panagiotopoulos A, Bariotakis M, et al. From Traditional Ethnopharmacology to Modern Natural Drug Discovery: A Methodology Discussion and Specific Examples. Molecules 2022; 27: 4060.
47. Domingo-Fernández D, Gadiya Y, Preto AJ, et al. Natural Products Have Increased Rates of Clinical Trial Success throughout the Drug Development Process. J Nat Prod 2024; 87: 1844–1851.
48. Smyth LA, Collins I. Measuring and interpreting the selectivity of protein kinase inhibitors. J Chem Biol 2009; 2: 131–151.
49. Uitdehaag JC, Verkaar F, Alwan H, et al. A guide to picking the most selective kinase inhibitor tool compounds for pharmacological validation of drug targets. Br J Pharmacol 2012; 166: 858–876.
50. Choo MZY, Chua JAT, Lee SXY, et al. Privileged natural product compound classes for anti-inflammatory drug development. Nat Prod Rep 2025; 42: 856–875.

Cite this article: Yudi A, Nia K, Ika K O, Eka Y R. LC–MS Profiling, In Silico Docking–MD and ADMET of *Uncaria gambir Roxb*. for p38 MAPK Inhibition. Pharmacogn J. 2026;18(1): 8-17.